

www.acsami.org Research Article

# Efficient Separation of Xylene Isomers by a Pillar-Layer Metal—Organic Framework

Liping Yang, Hanbang Liu, Danhua Yuan, Jiacheng Xing, Yunpeng Xu,\* and Zhongmin Liu



Cite This: https://doi.org/10.1021/acsami.1c10462



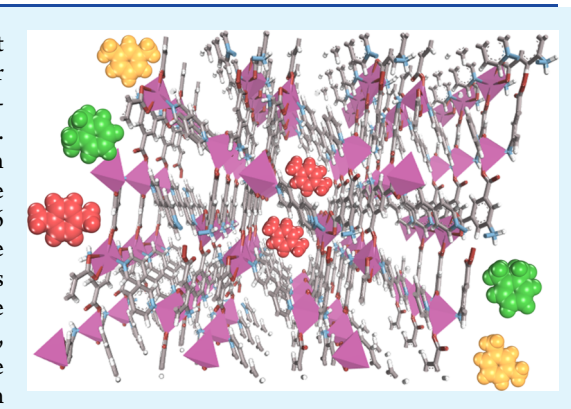
**ACCESS** 

Metrics & More



Supporting Information

**ABSTRACT:** The separation of xylene isomers is one of the most challenging issues in the chemical industry because of the similarity of their boiling points and kinetic diameters. This study focuses on the use of pillar-layer MOF-Co(aip)(bpy)<sub>0.5</sub> for adsorption and separation of xylene isomers. It was found that Co(aip)(bpy)<sub>0.5</sub> exhibited a significant *para*-selectivity in liquid-phase competitive adsorption of xylene isomers, and the competitive separation factors reached as high as 30 for *p*-xylene versus *m*-xylene and 16 for *p*-xylene versus *o*-xylene. Desorption experiments further confirmed the preferential adsorption of *p*-xylene on the adsorbent. Molecular simulations and calculations revealed that the order of interaction strengths for xylene molecules and the adsorbent framework was *p*-xylene  $\gg$  *o*-xylene, which illustrated the selective adsorption phenomena arising from the mechanism for microscopic interactions. This work broadens the application of pillar-layer MOF materials in the field of xylene isomer adsorption and separation.



KEYWORDS: pillar-layer materials, metal-organic frameworks, xylene separation, adsorption, competitive selectivity

#### 1. INTRODUCTION

Xylene isomers, including para-xylene (p-xylene), meta-xylene (m-xylene), and ortho-xylene (o-xylene), have different applications and values in the chemical industry. Among them, p-xylene is the key starting material for the production of refined terephthalic acid (PTA) and dimethyl terephthalate (DMT) that are further converted into various polyester products such as polyethylene terephthalate (PET) and polybutyl terephthalate (PBT).2 However, the similar kinetic diameters (6.5, 6.4, and 5.8 Å for o-xylene, m-xylene, and pxylene, respectively<sup>3,4</sup>) make them difficult to separate,<sup>5</sup> and the conventional distillation method is not suitable for the separation of *p*-xylene and *m*-xylene due to their similar boiling points (144.4, 139.1, and 138.4 °C for o-xylene, m-xylene, and p-xylene, respectively<sup>6</sup>). Therefore, the separation of xylene isomers is regarded as one of the seven world-challenging separations, and it is of great importance to develop an efficient and low-consumption method for xylene separation. In recent years, the continuous advances of adsorbent research have made the adsorptive separation method the most widely used separation method. At present, the majority of adsorbents for xylene separation are para-preferential adsorbents, whether in industrial applications or academic research.<sup>7,8</sup> Due to the lower composition for p-xylene in the mixed feed stream, it is usually easier to achieve high productivity using para-selective adsorbents.9 Current industrial adsorption techniques for the production of pure p-xylene are carried out with para-selective

faujasite-type zeolites using simulated moving bed technology 10,11 such as the commercial Parex process. 10,12 The separation is achieved using the differences in adsorption capacities for xylene isomers in the unique pore structure of cation-exchanged faujasite zeolites X or Y (BaX and KBaY). 9,13,14 After a long period of continuous improvement, the separation selectivity and the capacity of zeolites are still limited by the nature of the pore topology and cationic binding sites. It is still necessary to develop adsorbents with higher adsorption capacities and selectivities for the development of more efficient adsorption separation processes.

Compared with traditional zeolite adsorbents, metalorganic frameworks (MOFs) have shown unparalleled advantages and potential in the field of adsorption and separation due to their structural flexibility and tunability. One of the most promising applications of MOFs is in their use as xylene adsorbents. In fact, a vast number of MOFs have been studied for the adsorption and separation of xylene isomers, including *para*-selective MOFs, and they can achieve the separation of xylene isomers by pore size and the

Received: June 5, 2021 Accepted: August 23, 2021



interaction between their framework and p-xylene. For example, MIL-125 $^{16}$  and its derivative MIL-125-NH $_2^{17}$ preferentially adsorb p-xylene over m/o-xylene because of the stacking effect in the large octahedral cage combined with molecular sieving in the tetrahedron cage, and MIL-125-NH<sub>2</sub> exhibits excellent separation performance with a selectivity of 3 for p-xylene/m-xylene at 25 °C. Also, JUC-77<sup>18</sup> with twodimensional diamond-shaped channels is suitable for the passage of p-xylene with the smallest width. In addition, MAF-X8<sup>19</sup> selectively adsorbs p-xylene because its channel size and geometry allow commensurate stacking for p-xylene molecules, and this selectivity is comparable to BaX. MIL-47<sup>20</sup> also has an obvious separation effect on p-xylene/m-xylene with a selectivity of 2.9 at 25 °C. The study of MIL-47 in the separation of xylene isomers shows that the stacking effect produced by the  $\pi \cdots \pi$  interaction between the isomer molecules in MIL-47 is more conducive to the efficient packing of p-xylene. A more comprehensive comparison is given in Table S1, and it points out the methods used to derive the selectivities of these adsorbents. As shown in Table S1, the reported adsorption capacities of para-selective adsorbents for xylene isomers range from 10 to 50%, and the highest selectivity factor is approximately 10. Among the many kinds of MOFs, pillar-layer materials are currently a new type of three-dimensional network material and are regarded as one of the most promising materials; desirable performance is achieved by introducing a variety of pillars and linkers in three-dimensional frameworks for desired applications.<sup>21</sup> These emerging pillar-layer materials have been widely used in gas adsorption and separation, such as with carbon dioxide adsorption, <sup>22</sup>,23 methane-nitrogen separation, <sup>24</sup> and propylenepropane separation. 25,26

Herein, we present research on the xylene isomer adsorption and separation performance of cobalt-based pillar-layered MOF-Co(aip)(bpy)<sub>0.5</sub>. Single-component and binary-component competitive adsorptions of xylene isomers were investigated in the liquid phase at room temperature. The gas-phase adsorption and desorption processes of p-xylene/m-xylene or p-xylene/o-xylene mixtures were studied by temperature-programmed desorption (TPD) experiments. p-Xylene/m-xylene or p-xylene/o-xylene liquid-phase adsorption and gasphase desorption experiments were designed to verify the selective adsorption performance of Co(aip)(bpy)<sub>0.5</sub>. Finally, molecular simulations and theoretical calculations were carried out to reveal the microscopic mechanism of the highly selective adsorption of p-xylene.

## 2. EXPERIMENTAL SECTION

**2.1. Materials.** p-Xylene ( $C_8H_{10}$ , 99.0%, Aladdin), o-xylene ( $C_8H_{10}$ , 99.0%, Aladdin), m-xylene ( $C_8H_{10}$ , 99.0%, Aladdin), n-heptane ( $C_7H_{16}$ , 99.5%, Tianjin Damao Chemical Reagent), cobalt acetate tetrahydrate ( $C_9(CH_3COO)_2$ - $4H_2O$ , 99.5%, Aladdin), 4,4′-bipyridine ( $C_{10}H_8N_2$ , 98%, Aladdin), 5-aminoisophthalic acid ( $C_8H_7NO_4$ , 98%, Aladdin), and methanol ( $CH_4O$ , 99.5%, Tianjin Damao Chemical Reagent) were commercially purchased and used without further purification.

**2.2. Preparation of Adsorbent.** The preparation of Co(aip)-(bpy) $_{0.5}$  was performed as previously reported. Typically, 2.2982 g of Co(CH $_3$ COO) $_2$ ·4H $_2$ O was dissolved in 80 mL of deionized water at room temperature. Also, the mixed solution 0.6246 g of 4,4′-bipyridine and 1.4496 g of 5-aminoisophthalic acid in 80 mL of methanol was added to the above solution. Then, the mixed solution was stirred and sonicated until evenly homogenous and was placed in a 200 mL Teflon liner autoclave at 60 °C for 72 h. The purple product

was filtered, washed with deionized water and methanol, and was immersed in methanol solvent for 3 days during which the supernatant was replaced by fresh methanol three times. Purple samples were then transferred to a Micromeritics ASAP 2020 degas port and evacuated at 150  $^{\circ}\mathrm{C}$  for 8 h for further adsorption tests.

**2.3. Characterizations.** The powder X-ray diffraction (PXRD) patterns were collected on a PANalytical X'Pert PRO X-ray diffractometer using the Cu  $K\alpha$  radiation ( $\lambda$  = 1.54059 Å), operating at 40 kV and 40 mA and the scanning speed was 5°/min in the 2θ range from 5 to 60°. Thermogravimetric analyses (TGA) were conducted on an SDT Q600 (TA Instruments-Waters LLC, USA) from room temperature to 800 °C with a heating rate of 5 °C/min in a N<sub>2</sub> flow of 100 mL/min. The temperature-programmed desorption (TPD) experiments were carried out with the chemical adsorption instrument (Micromeritics, ASAP-2920, USA) to determine the xylene desorption. The CO<sub>2</sub> adsorption isotherm was measured by a volumetric adsorption apparatus (Micromeritics, Germini VII 2390, USA). Sorption kinetic measurements were conducted at 25 °C using an intelligent gravimetric analyzer (IGA) (Hiden Isochema, IGA100).

2.4. Gas Chromatography Analysis Conditions. All GC analyses were carried out on an Agilent 7890A instrument equipped with a flame ionization detector (FID), and the GC column used was a DB-FFAP capillary column (30 m  $\times$  0.32 mm  $\times$  0.25  $\mu$ m). The GC conditions were as follows: column temperature of 45 °C (2 min hold) to 60 °C at 5 °C/min and then to 150 °C at 20 °C/min and cooled down to 45 °C; injection temperature: 180 °C; detection temperature: 200 °C. Each liquid sample (0.1  $\mu$ L) was injected through the GC inlet with a split ratio of 60:1. Three injections per sample were performed to determine average retention times and areas. Chemstation software (Agilent Technologies) was used for system operation and data acquisition.

**2.5.** Solid–Liquid Adsorption–Desorption Experiments. 2.5.1. Batch Experiments. For single-component batch experiments at 25 °C, similar to the reported literature procedure, <sup>17</sup> a centrifuge tube with 0.1 g of pretreated adsorbent and an empty reference tube were contained with 1 g of xylene isomer solution in n-heptane. The sorption solutions were filtered through a lipophilic Nylon66 filter (0.22  $\mu$ m) prior to injection. Uptakes from solution were directly obtained after 2.5 h by gas chromatography (GC) output data. Adsorption uptakes  $q_t$  were calculated using eq 1:

$$q_t = \frac{(c_0 - c_t)}{m} \tag{1}$$

where  $c_0$  and  $c_t$  (wt %) are the initial mass fraction of the single-component isomer in xylene mixtures and the mass fraction when sampling to analyze, respectively. m (g) is the mass of the adsorbent used in the adsorption experiment.

The single-component adsorption isotherms were fitted by a Langmuir model. The model equation can be expressed as follows:

$$q_{e} = \frac{q_{m}bc}{1+bc} \tag{2}$$

where  $q_e$  is the amounts adsorbed of an adsorbent in equilibrium (mg/g), c is the equilibrium concentration (wt %),  $q_m$  is the saturated adsorption capacity of the monolayer (mg/g), and b is the adsorption equilibrium constant.

By testing the adsorption isotherms at different temperatures (25, 35, and 50 °C), the adsorption enthalpy ( $\Delta H_s$ ) was calculated based on the Clausius—Clapeyron equation:

$$\ln(P) = \frac{\Delta H_s}{RT} + C \tag{3}$$

The slope of  $\ln(P)$  versus 1/T was calculated to obtain the  $\Delta H_{\rm s}$ . For competitive batch adsorption experiments, equimolar mixtures of xylene isomers were used; the detection method is the same as the single-component experiment described above. Selectivities  $\alpha_{ij}$  were calculated using eq 4:

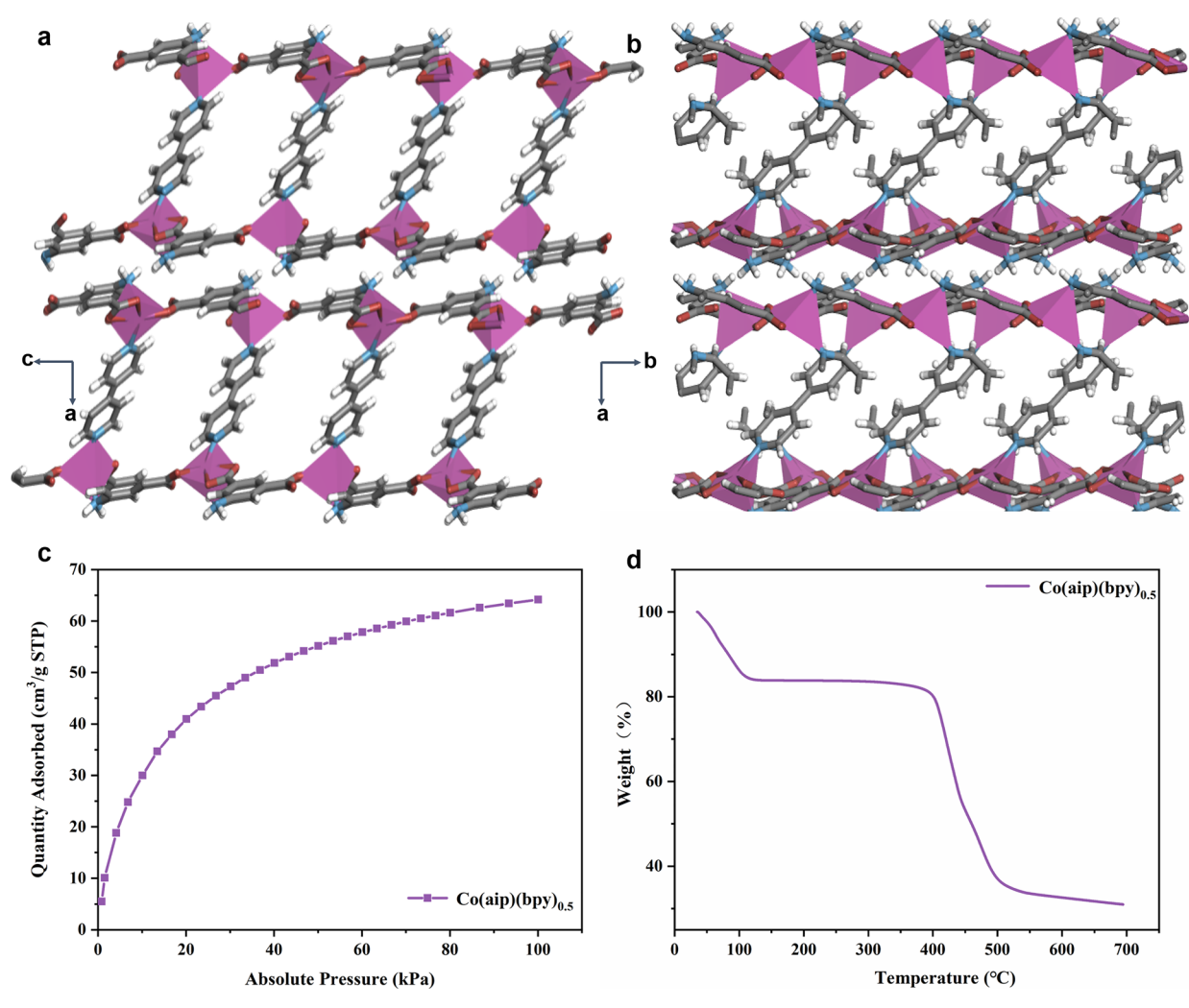


Figure 1. (a,b) View of the pillar-layer structures of  $Co(aip)(bpy)_{0.5}$  along the b axis in (a) and c axis in (b). (c)  $CO_2$  adsorption isotherm of  $Co(aip)(bpy)_{0.5}$  at 0 °C. (d) TGA curve of synthesized  $Co(aip)(bpy)_{0.5}$  under a  $N_2$  atmosphere.

$$\alpha_{ij} = \left(\frac{q_i}{q_j}\right) \times \left(\frac{c_j}{c_i}\right) \tag{4}$$

where  $q_i$  and  $q_j$  (mg/g) are the uptakes of the one-component xylene isomers i and j adsorbed per gram of adsorbent. Also,  $c_i$  and  $c_j$  (wt %) are the mass fraction of the isomers i and j in the external liquid phase.

2.5.2. Liquid-Phase Adsorption and Gas-Phase Desorption Experiments. The specific experimental process was designed as follows: About 5 g of the pretreated adsorbent was added to 10 g of nheptane mixed adsorption solution containing p-xylene/m-xylene (10:1 or 1:1). After stirring and adsorbing for 24 h, the saturated adsorbent was suction filtered with n-heptane, and the filter cake was soaked in the *n*-heptane solvent. This step was repeated three times until the adsorption liquid outside the adsorbent framework was washed out. Then, the filter cake of the last suction filtration was loaded into the desorption column for purging with nitrogen at a flow rate of 100 mL/min for 5 h at 50 °C, and the adsorbent was heated to 300  $^{\circ}\text{C}$  for desorption for 1 h, and the desorbed components were collected with 10 g of cooled n-heptane solvent at the end of the adsorption column outlet. After the desorption process, the collected solutions were tested by GC for the content of xylene components and compared with the chromatographic data of the initial adsorption solution before the adsorption process.

2.5.3. Breakthrough Experiments. Liquid-phase dynamic breakthrough experiments were carried out following the reported literature at 25 °C. <sup>17</sup> A hand-made column (L = 50 mm, D = 4 mm) was

packed with approximately 0.5 g of degassed pelletized adsorbent. Then, the column was pumped with binary equimolar feed solution using n-heptane as solvent (p-xylene/m-xylene: 1 wt %) at 0.5 mL/min, and the effluents were monitored by gas chromatography.

**2.6.** Solid-Vapor Adsorption-Desorption Experiments. 2.6.1. Vapor-Phase Desorption Experiments. Xylene vapor (p-xylene and m-xylene) was introduced into the adsorbent bed filled with the pretreated desolvent sample by the steam generator set up through the He gas flow until the adsorbent was saturated, and the obtained sample was subsequently subjected to the thermal analysis experiments. Vapor-phase desorption experiments were conducted on a SDT Q600. Samples were placed in open ceramic pans with an empty ceramic pan functioning as a reference. Also, nitrogen was used as purge gas at the flow of 100 mL/min. The ramp rate was 10 °C/min from room temperature to approximately 300 °C.

2.6.2. Temperature-Programmed Desorption (TPD). The desorption of p-xylene, m-xylene, and their binary mixtures adsorbed in pelletized  $Co(aip)(bpy)_{0.5}$  were studied by TPD in a low-vacuum system equipped with a steam generator. After opening the sealed tube, the adsorbent sample (40–60 mesh) was placed in a narrow quartz reactor, and any residual solvent ( $H_2O$  and methanol) was removed by passing dry argon over the sample and heating up to 200 °C for half an hour for the pretreatment process. Then, the reactor was cooled to 50 °C, and continuous pulse injections were performed until adsorption is saturated. The sample was then heated at a constant rate of 10 °C/min from 50 to 300 °C, and the desorption of xylene adsorbates was recorded in the whole desorption process using

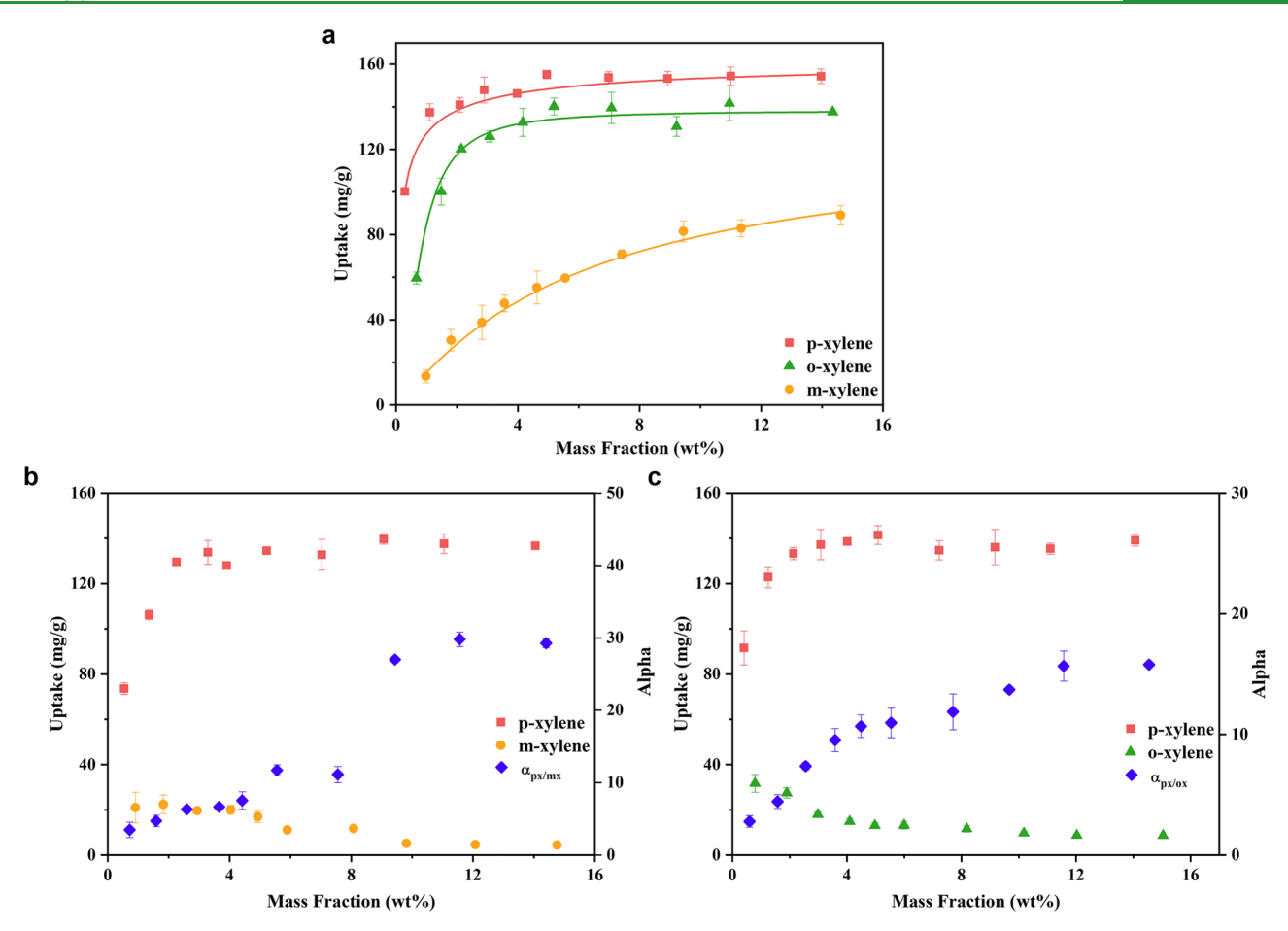


**Figure 2.** (a) Single-component batch adsorption experiments and (b, c) binary-component competitive adsorption experiments for p-xylene (squares), m-xylene (circles), and o-xylene (triangles) on  $Co(aip)(bpy)_{0.5}$  at 25 °C: uptake (mg/g) vs equilibrium mass fraction (wt %). The selectivities alpha  $(\alpha)$  are given with the right axis in panels b and c. Error bars are within the sizes of the symbols.

a thermal conductivity detector (TCD) to detect the xylene desorption signal. Samples weighing approximately 150 mg were used for each TPD run.

2.6.3. Sorption Kinetics (IGA). About 40–60 mg of the pelletized adsorbent sample (40–60 mesh) was degassed at 200 °C for more than 6 h. Afterward, the adsorption test of three xylene isomers was carried out under the conditions of 25 °C and 1.3 mbar. The data obtained as mass vs time were used to calculate the diffusional time constants. Diffusional time constants  $(D/r^2)$  were calculated by the short-time solution of the diffusion equation.<sup>29</sup>

$$\frac{q_t}{q_\infty} = \frac{6}{\sqrt{\pi}} \sqrt{\frac{D}{r^2} \times t} \tag{5}$$

where  $q_i$  is the adsorbed amount at time t,  $q_\infty$  is the adsorbed amount at equilibrium, r is the radius of the equivalent spherical particle, and D is the diffusivity.

**2.7. Molecular Simulation Details.** The host—guest interaction energies were calculated from the density functional theory (DFT) calculations using the Materials Studio (version 6.0) DMol3 Module. The DFT calculations were performed using the Perdew—Burke—Ernzerhof (PBE) exchange-correlation functional within the generalized gradient approximation (GGA). The set optimization convergence standard SCF tolerance value was 0.001 meV/atom. At the same time, the max SCF cycles was found to be 300 during the calculation process. First, the conformational geometries of the adsorbent and all adsorbates *p*-xylene, *m*-xylene, and *o*-xylene were optimized before calculation. Then, three optimized xylene isomer molecules were introduced into the framework of the adsorbent framework, respectively, using the Forcite

Module. Finally, the calculation formula for the interaction energy between adsorbate molecules and  $Co(aip)(bpy)_{0.5}$  adsorbent is

$$\Delta E = E(\text{adsorbent} + \text{xylene isomer}) - E(\text{adsorbent})$$
$$- E(\text{xylene isomer}) \tag{6}$$

The smaller  $\Delta E$  value indicates stronger adsorption. It is worth noting that the calculated interaction energies cannot be quantitatively correlated with the actual experiments; however, it can predict the trend of the possible results. At the same time, molecular electrostatic potential analyses of optimized  $\text{Co(aip)(bpy)}_{0.5}$ , xylene isomers, and complexes were conducted also using the PBE exchange-correlation functional within the GGA in Dmol3 Module.<sup>32</sup>

# 3. RESULTS AND DISCUSSION

As shown in Figure 1a,b, the layers in the network structure of the synthesized adsorbent are connected by interlayer hydrogen bonds. In each the one-dimensional channel, intralayer interactions including  $\pi\cdots\pi$  stacking and  $C-H\cdots\pi$  interaction are formed between the adjacent 5-aminosophthalic acid (aip) and pyridine rings of 4,4′-bipyridine (bpy) ligands. In the characterization of the pore structure, we found that there was almost no  $N_2$  adsorbed for these samples at  $-196~^{\circ}\mathrm{C}^{24}$  and that the adsorption performance of its pores can be quantitatively characterized by a  $\mathrm{CO}_2$  adsorption isotherm, which is consistent with the reported literature.  $^{23}$  TGA was carried out to investigate to the thermal stability of the adsorbent. As shown in Figure 1d, the TGA curve had two

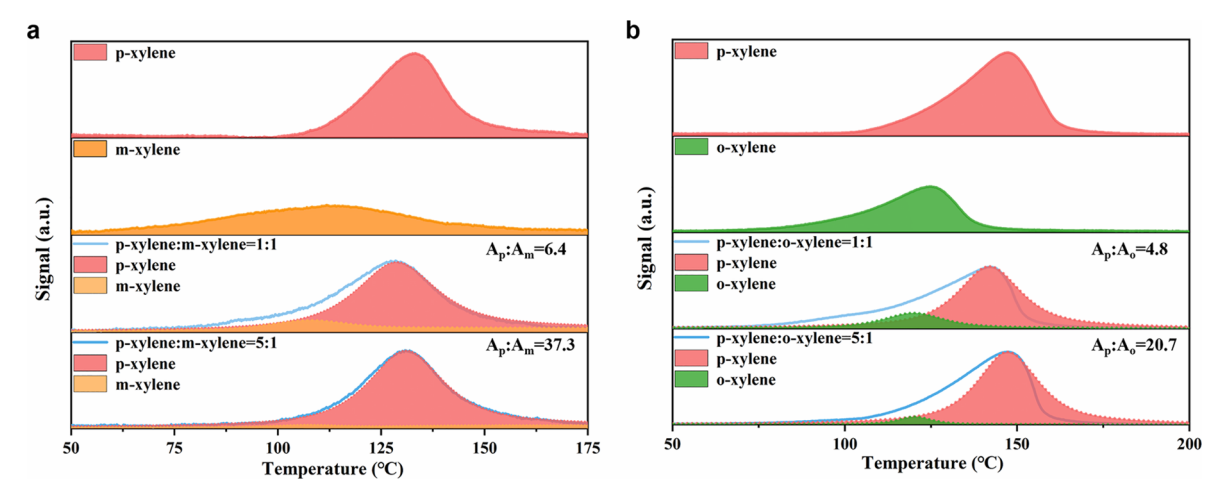


**Figure 3.** TPD profiles of (a) *p*-xylene/*m*-xylene and (b) *p*-xylene/*o*-xylene adsorbed on Co(aip)(bpy)<sub>0.5</sub> after individual adsorption and coadsorption. The bottom two peaks of the mixed components were processed by peak splitting, and their peak area ratios are marked.

obvious weight loss: the first weight loss peak occurred between 30 and 120 °C, which is related to the removal of residual guest solvents in the pores of the adsorbent, and the second step of weight loss occurred at 400–550 °C, which is assigned to decomposition of the pillar-layer structure. The above results revealed that this material has a stable structure and good thermal stability. In addition, other relevant structural characterizations of the synthesized Co(aip)(bpy)<sub>0.5</sub> adsorbent are shown in the Supporting Information. The results of FT-IR and XRD experiments both proved that the adsorbent material was successfully prepared and that the adsorbent material had a certain degree of crystallinity.

Liquid-phase batch adsorption experiments were used to evaluate the adsorption performance of this material. From the single-component adsorption isotherms shown in Figure 2a, it demonstrated that the Co(aip)(bpy)<sub>0.5</sub> pillar-layer adsorbent had the largest adsorption capacity for p-xylene, and the pxylene uptake quickly reached a plateau at 156 mg/g and uptakes of o-xylene and m-xylene were lower. The adsorption capacities for the three isomers increased as their concentrations in the adsorption solution increased and reached adsorption saturation, but it is obvious that p-xylene and oxylene reached adsorption saturation at lower concentrations. The adsorbent exhibited the weakest adsorption capacity for m-xylene, with an adsorption capacity of 90 mg/g at a 15 wt % concentration, and the isotherm of m-xylene did not reach adsorption saturation in the tested concentration range. The Langmuir adsorption model was used to fit the isotherms for single-component batch adsorption (Table S2). In addition, we noticed that o-xylene has the largest molecular size among xylene isomers, but its adsorption capacity was significantly higher than that of m-xylene, which has a slightly smaller size. Therefore, we reasonably believe that the adsorption difference of this adsorbent is not entirely caused by the pore size sieving effect,<sup>33</sup> operating in MIL-125,<sup>16</sup> MIL-125-NH<sub>2</sub>,<sup>17</sup> Cu-(CDC),<sup>34</sup> and JUC-77,<sup>18</sup> but is probably due to the unique interaction between the isomer molecules and the adsorbent after effective packing in the adsorbent; this is seen, for example, in faujasite zeolites, 35,36 MIL-47,20 and MAF-X8.19 By testing the adsorption isotherms of the xylene isomers at different temperatures, the adsorption enthalpies were calculated and are shown in Table S3. The adsorption enthalpies of the three isomers were all negative, indicating that the adsorption process was exothermic. Also, *p*-xylene was more negative than *o*-xylene and *m*-xylene; that is, the absolute value of the adsorption enthalpy of *p*-xylene was the largest followed by *o*-xylene, and *m*-xylene was the smallest, indicating that the interaction between *p*-xylene and the adsorbent was stronger. The order of calculated adsorption enthalpy of the three isomers was consistent with the adsorption uptake obtained in the above single-component adsorption experiment.

The isotherms for binary-component competitive adsorption by  $Co(aip)(bpy)_{0.5}$  are shown in Figure 2b,c. When p-xylene and m-xylene were coadsorbed, the adsorption capacity of pxylene still reached adsorption saturation at a lower concentration, which is consistent with the behavior in single-component adsorption, and the saturated adsorption capacity was as high as 136 mg/g. However, the adsorption behavior of *m*-xylene in the presence of *p*-xylene was obviously different from that in the single-component experiment. With increasing adsorption concentration, the adsorption capacity for m-xylene gradually decreased, its absorption capacity was never higher than 20 mg/g, and the p-xylene/m-xylene selectivity was as high as 30. In addition, a similar competitive adsorption phenomenon was observed in the coadsorption of p-xylene and o-xylene. As shown in Figure 2c, p-xylene maintained a relatively high adsorption capacity, and the saturated adsorption capacity was 139 mg/g. The adsorption trend for o-xylene was similar to that of m-xylene, and the adsorption capacity continued to decrease as the concentration increased. However, the adsorption capacity of o-xylene was slightly higher than that of *m*-xylene, which is in line with the fact that the adsorption capacity of o-xylene in singlecomponent adsorption was higher than that of m-xylene. As shown in Figure 2b,c, the results of binary-component competitive adsorption suggested that the adsorption preference of  $Co(aip)(bpy)_{0.5}$  for p-xylene strongly increased with the increasing external bulk phase concentration, which further showed that this isomer is more likely to pack in adsorbent pores. In other words, the adsorption of *p*-xylene inhibited the uptake of o-xylene and m-xylene, and p-xylene was clearly the preferentially adsorbed component, which is consistent with the competitive adsorption phenomenon mentioned in the literature studies. 2,20 At the same time, Co(aip)(bpy)0.5 exhibits a competitive separation performance that outper-

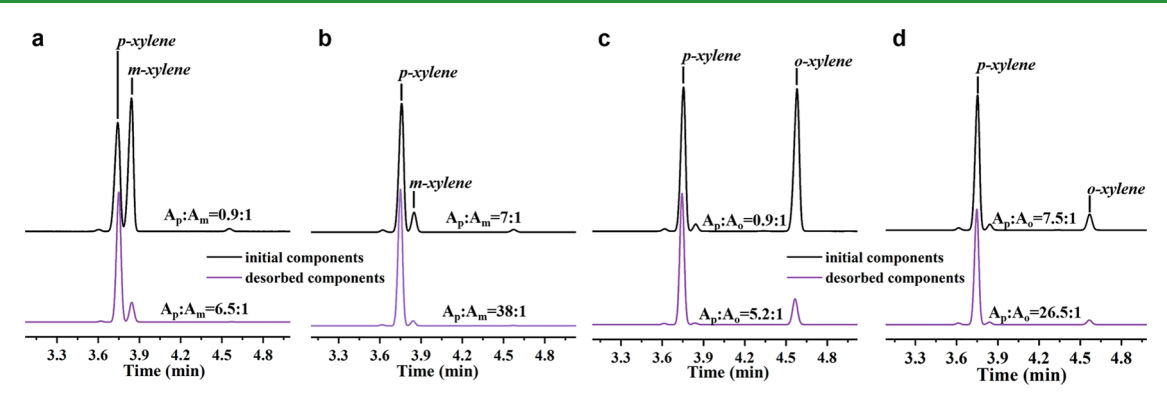


**Figure 4.** Chromatograms of the initial components (adsorption solution) and desorbed components (collected solution from desorption). The concentrations of the initial adsorption solutions were (a) *p*-xylene:*m*-xylene = 1:1, (b) *p*-xylene:*m*-xylene = 10:1, (c) *p*-xylene:*o*-xylene = 1:1, and (d) *p*-xylene:*o*-xylene = 10:1. The ratios of chromatographic peak area percentages of initial components and desorbed components are marked. Due to the different response values for the xylene isomers with the chromatographic detector, there was a slight difference between the initial solution ratio and the peak area percentage ratio.

forms the majority of those for the summarized porous adsorbents. Moreover, in order to further verify superior adsorption performance for p-xylene over m-xylene, we carried out the liquid-phase breakthrough experiment in Figure S6 and the breakthrough curve showed a slow equilibration of p-xylene and m-xylene. It can be seen intuitively that m-xylene first eluted and p-xylene was detected subsequently in the effluent, which means that the adsorbent has a higher priority to adsorb p-xylene than m-xylene. However, during the entire breakthrough experiment, both m-xylene and p-xylene took a long time to reach adsorption saturation. Through the adsorption kinetic experiment and the calculations of diffusion time constants, we speculated that the cause of this phenomenon is the different diffusion rates of p-xylene and m-xylene (Figure S8 and Table S4). The diffusion time constant of *m*-xylene was much smaller than that of p-xylene, which indicated that mxylene had obvious diffusion limitation on the adsorbent. Therefore, it took longer for m-xylene to reach adsorption saturation. At the same time, because p-xylene had strong competition with m-xylene, it can continuously replace mxylene from the adsorption site on the adsorbent, subsequently p-xylene slowly reached equilibrium. For these reasons, the adsorbent exhibits an absolute advantage in adsorbing *p*-xylene.

Temperature-programmed desorption (TPD) experiments provided insights into the adsorption and desorption performance of the adsorbent and the adsorption difference for pxylene/m-xylene and p-xylene/o-xylene. The inert gas argon was used to bring xylene (single- or binary-component) in the steam generator into the quartz tube containing the adsorbent. Continuous pulse injections were carried out at 50 °C until the adsorbent reached saturation and began to heat up and desorb. The desorption profiles for different experimental conditions are shown in Figure 3. The single-component gas desorption profile indicated that the desorption peak position for *p*-xylene exhibited a higher temperature and a larger peak area than mxylene and o-xylene, which means that the adsorbent had a stronger adsorption interaction and a higher adsorption capacity for p-xylene compared to m-xylene and o-xylene. This is consistent with the trends of the above liquid-phase adsorption results. It is noteworthy that the boiling point of pxylene (138.4 °C) is lower than those of m-xylene (139.1 °C) and o-xylene (144.4 °C), but the desorption temperature is higher, which indicates that the interaction between the adsorbent and p-xylene is indeed stronger than those of mxylene and o-xylene, thus showing the high priority for p-xylene under competitive adsorption conditions. This feature can be used to distinguish the peaks from mixed gas desorption. Vapor desorptions of xylene mixtures with different compositions were also investigated. When the contents of p-xylene and m-xylene or o-xylene were equal, two obvious desorption peaks were observed, and we performed mathematical fitting of the obtained desorption peaks and integrated the fitted peaks to obtain peak area ratios. The desorption temperature of the single-component desorption experiment suggested that among the desorption peaks for mixed components, the desorption peak with the higher temperature was that for desorption of p-xylene. The corresponding peak area was also significantly higher than those of the m-xylene and o-xylene components, and the peak area ratios of p-xylene/m-xylene and p-xylene/o-xylene were 6.4 and 4.8, respectively. After increasing the content ratios of p-xylene/m-xylene or pxylene/o-xylene to 5:1, the desorption peak areas for m-xylene or o-xylene were greatly reduced, which means that the adsorption of p-xylene inhibited the coadsorption of m-xylene or o-xylene. The peak area ratios of p-xylene/m-xylene and pxylene/o-xylene increased to 37.3 and 20.7, respectively, which is in accordance with the results of liquid-phase competitive adsorption experiments.

In addition, p-xylene/m-xylene and p-xylene/o-xylene binary-component liquid-phase adsorption and gas-phase desorption experiments were designed to further verify the competitive adsorption performance of this adsorbent. The pretreated adsorbent sample was put into a solution of xylene mixture diluted with *n*-heptane to achieve saturated adsorption. Then, the adsorbent was washed with *n*-heptane and filtered until the xylene component outside the adsorbent framework was eliminated. The filter cake was heated under a nitrogen atmosphere, and the desorbed components were absorbed with the *n*-heptane solvent. The results of chromatographic analysis of the *n*-heptane absorption solution are shown in Figure 4. It can be seen from the chromatograms that the peak area ratios of p-xylene/m-xylene and p-xylene/o-xylene for the xylene mixtures obtained by desorption were significantly higher than those of the initial adsorption solution. For p-xylene and mxylene mixtures, when the initial peak area ratio of p-xylene/mxylene was 0.9, the peak area ratio of p-xylene/m-xylene in the desorption products was increased to 6.5, and when the initial peak area ratio of p-xylene/m-xylene was 7, the final peak area

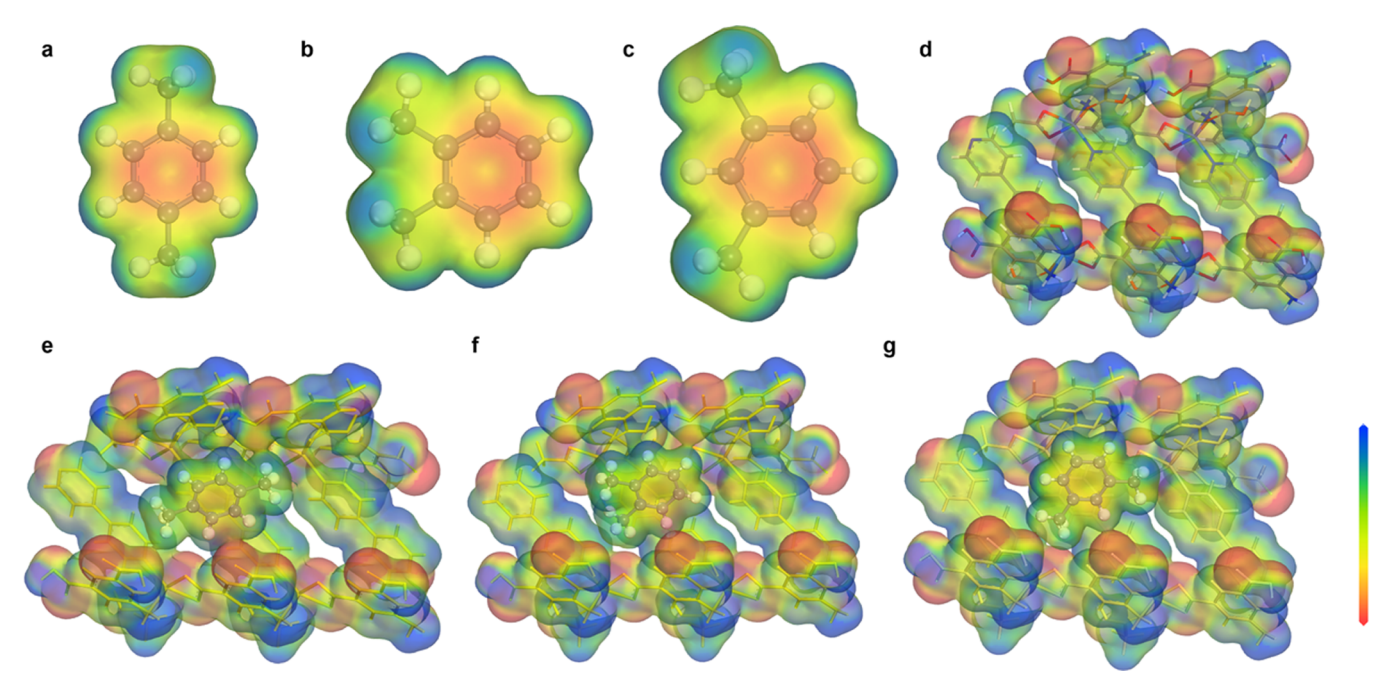


**Figure 5.** Molecular electrostatic potentials of (a) p-xylene, (b) o-xylene, (c) m-xylene, (d)  $Co(aip)(bpy)_{0.5}$ , (e)  $Co(aip)(bpy)_{0.5}-p$ -xylene, (f)  $Co(aip)(bpy)_{0.5}-o$ -xylene, and (g)  $Co(aip)(bpy)_{0.5}-m$ -xylene complexes are mapped using a spectrum of colors. The regions with the red color represent the highest electron density, while the blue color represents regions with the lowest electron density.

ratio of p-xylene/m-xylene for desorption products was as high as 38. When the initial peak area ratios of p-xylene/o-xylene were 0.9 and 7.5 for p-xylene and o-xylene mixtures, the peak area ratios of p-xylene/o-xylene for desorption products increased to 5.2 and 26.5, respectively. The above data show that the pillar-layer adsorbent had a significant effect in the purification of xylene mixtures and indicates prospects for application in xylene isomer separation.

The previous adsorption results showed that the Co(aip)-(bpy)<sub>0.5</sub> adsorbent shows high selectively for p-xylene adsorption under competitive adsorption conditions. In the following work, molecular simulations and calculations were carried out to explain the different adsorption selectivities for xylene isomers on the pillar-layer adsorbent. First, molecular electrostatic potentials were obtained to determine the electron density distributions and interactions.<sup>32</sup> The molecular electrostatic potentials of the Co(aip)(bpy)<sub>0.5</sub> framework, xylene isomers, and complexes were derived from density functional theory (DFT) calculations using the GGA/PBE level of theory.<sup>31</sup> Different properties for electrostatic potential are illustrated by different colors. As seen from the maps of xylene isomers (Figure 5a-c), the center of the benzene ring possessed the highest electron density. The phenyl ring of xylene isomers experienced a reduction in electron density when complexed with the adsorbent framework (Figure 5e-g). This implied that there was an electron transfer interaction between the adsorbent framework and adsorbate molecules. Then, we used the calculated interaction energies  $(\Delta E)$  to further illustrate the difference in interactions between these three isomers with the adsorbent framework, as shown in Figure 6a. 30,37 A smaller  $\Delta E$  value indicated stronger adsorption and a more stable configuration after adsorption. The conformational geometries of all adsorbate molecules and the Co(aip)(bpy)<sub>0.5</sub> adsorbent were optimized before calculation. The order of the  $\Delta E$  for xylene molecules and adsorbent is p-xylene  $\ll$  o-xylene  $\approx$  m-xylene, which is consistent with the

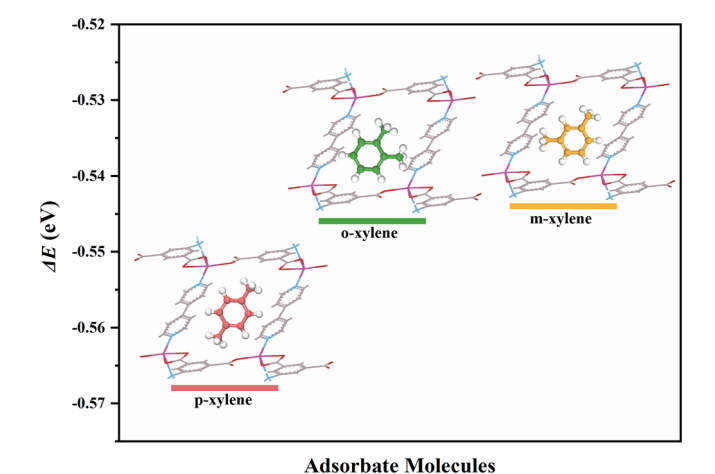


**Figure 6.** Schematic diagram of interaction energies for the xylene isomers with  $Co(aip)(bpy)_{0.5}$  (a selected channel in the  $Co(aip)(bpy)_{0.5}$  framework and three isomers as illustrated. Red: *p*-xylene; green: *o*-xylene; and yellow: *m*-xylene).

preferences seen in the aforementioned liquid-phase adsorption experiment results. The  $\Delta E$  between p-xylene and the adsorbent was much lower than those for the other two isomers, which proved that the adsorbent has the strongest binding capacity with p-xylene and that the adsorbed configuration was more stable, which is beneficial in allowing more p-xylene to adsorb and pack easily inside the pores. This energy trend was consistent with the calculated results of the adsorption enthalpy and further explained the manifested inhibitory effect of p-xylene on the other two isomers during competitive adsorption.

By combining experimental results and guidance from theoretical calculations, speculation on the mechanism for competitive adsorption is proposed in Figure S14. Under single-component adsorption conditions, *p*-xylene, *o*-xylene,

and *m*-xylene can bind to the adsorption sites on the adsorbent, but the binding abilities of *m*-xylene and *o*-xylene were relatively weak, which led to the highest uptake for *p*-xylene among the isomers. For binary-component competitive conditions, all isomer molecules exhibited a certain degree of adsorption at low concentrations. However, as the concentration increased, *p*-xylene, which has a lower binding energy and stronger adsorption, bound with the adsorption sites occupied by *m*-xylene or *o*-xylene on the adsorbent, gradually replacing *m*-xylene or *o*-xylene and causing the competitive adsorption selectivity to increase gradually with concentration. This superior adsorption capacity and strong affinity for *p*-xylene gives the adsorbent great potential in the field of xylene isomer adsorption and separation.

# 4. CONCLUSIONS

In conclusion, the performance of the pillar-layer material  $Co(aip)(bpy)_{0.5}$  in the separation of xylene isomers was systematically investigated by adsorption and desorption experiments as well as with theoretical calculations. It was found that the priority order for adsorption of xylene isomers on the adsorbent is p-xylene  $\gg$  o-xylene  $\approx$  m-xylene. The adsorbent showed an absolute preference for p-xylene in competitive adsorption of xylene isomers and exhibited ultrahigh competitive selectivity for p-xylene over m-xylene and o-xylene. The competitive separation factors of p-xylene versus m-xylene and p-xylene versus o-xylene reached as high as 30 and 16, respectively. Molecular simulations and calculations revealed that the pores of Co(aip)(bpy)<sub>0.5</sub> provide a chemical environment more suitable for hosting p-xylene than the other two isomers, m-xylene and o-xylene, which also provides inspiration for finding other efficient pillar-layer material adsorbents for xylene isomer separation. The pillar-layer  $MOF-Co(aip)(bpy)_{0.5}$  exhibits outstanding separation performance and could potentially be an adsorbent for practical application in xylene isomer adsorptive separation. This work enables this series of pillar-layer materials to open up great potential in the field of xylene isomer adsorption and separation.

# ASSOCIATED CONTENT

# Supporting Information

The Supporting Information is available free of charge at https://pubs.acs.org/doi/10.1021/acsami.1c10462.

PXRD, FT-IR, TGA, the breakthrough curve, the breakthrough setup, sample photos, SEM images, sorption kinetics results, adsorption isotherms of xylene isomers at different temperatures, quaternary- and ternary-component adsorption isotherms, a summary of para-selective adsorbents, fitting parameters of the Langmuir adsorption model, the adsorption enthalpy, diffusion time constant, interaction energies of simulation (PDF)

# AUTHOR INFORMATION

# **Corresponding Author**

Yunpeng Xu — National Engineering Laboratory for Methanol to Olefins, Dalian National Laboratory for Clean Energy, Dalian Institute of Chemical Physics, Chinese Academy of Sciences, Dalian 116023, China; □ orcid.org/0000-0002-5165-5803; Email: xuyunpeng@dicp.ac.cn

#### **Authors**

Liping Yang — National Engineering Laboratory for Methanol to Olefins, Dalian National Laboratory for Clean Energy, Dalian Institute of Chemical Physics, Chinese Academy of Sciences, Dalian 116023, China; University of Chinese Academy of Sciences, Beijing 100049, China

Hanbang Liu — National Engineering Laboratory for Methanol to Olefins, Dalian National Laboratory for Clean Energy, Dalian Institute of Chemical Physics, Chinese Academy of Sciences, Dalian 116023, China; University of Chinese Academy of Sciences, Beijing 100049, China

Danhua Yuan – National Engineering Laboratory for Methanol to Olefins, Dalian National Laboratory for Clean Energy, Dalian Institute of Chemical Physics, Chinese Academy of Sciences, Dalian 116023, China

Jiacheng Xing — National Engineering Laboratory for Methanol to Olefins, Dalian National Laboratory for Clean Energy, Dalian Institute of Chemical Physics, Chinese Academy of Sciences, Dalian 116023, China; University of Chinese Academy of Sciences, Beijing 100049, China

Zhongmin Liu — National Engineering Laboratory for Methanol to Olefins, Dalian National Laboratory for Clean Energy, Dalian Institute of Chemical Physics, Chinese Academy of Sciences, Dalian 116023, China; University of Chinese Academy of Sciences, Beijing 100049, China; orcid.org/0000-0002-7999-2940

Complete contact information is available at: https://pubs.acs.org/10.1021/acsami.1c10462

### **Author Contributions**

The manuscript was written through contributions of all authors. All authors have given approval to the final version of the manuscript. L.Y. synthesized the adsorbents and performed the relevant characterizations and liquid-phase adsorption experiments in this work. H.L. and L.Y. calculated interaction energies and molecular electrostatic potentials. Y.X., D.Y., L.Y., and J.X. participated in project planning and discussions of the results. Y.X. and Z.L. conceived and supervised the research project. All authors helped in writing the paper and commented on it.

#### **Notes**

The authors declare no competing financial interest.

# ACKNOWLEDGMENTS

This research was supported by the National Natural Science Foundation of China (no. 21802136) and the Talent Program for Revitalization of Liaoning Province (XLYC1905017). We highly appreciate Yanli He and Yijun Zheng (Dalian Institute of Chemical Physics) for the assistance in the vapor-phase thermal analysis experiments.

# REFERENCES

- (1) Sholl, D. S.; Lively, R. P. Seven Chemical Separations to Change the World. *Nature* **2016**, *532*, 435–437.
- (2) Alaerts, L.; Maes, M.; Giebeler, L.; Jacobs, P. A.; Martens, J. A.; Denayer, J. F. M.; Kirschhock, C. E. A.; De Vos, D. E. Selective Adsorption and Separation of ortho-Substituted Alkylaromatics with the Microporous Aluminum Terephthalate MIL-53. *J. Am. Chem. Soc.* **2008**, *130*, 14170–14178.
- (3) Yang, Y.; Bai, P.; Guo, X. Separation of Xylene Isomers: A Review of Recent Advances in Materials. *Ind. Eng. Chem. Res.* **2017**, 56, 14725–14753.

- (4) Sapianik, A. A.; Dudko, E. R.; Kovalenko, K. A.; Barsukova, M. O.; Samsonenko, D. G.; Dybtsev, D. N.; Fedin, V. P. Metal-Organic Frameworks for Highly Selective Separation of Xylene Isomers and Single-Crystal X-ray Study of Aromatic Guest-Host Inclusion Compounds. ACS Appl. Mater. Interfaces 2021, 13, 14768–14777.
- (5) Peralta, D.; Chaplais, G.; Paillaud, J.-L.; Simon-Masseron, A.; Barthelet, K.; Pirngruber, G. D. The Separation of Xylene Isomers by ZIF-8: A Demonstration of the Extraordinary Flexibility of the ZIF-8 Framework. *Microporous Mesoporous Mater.* **2013**, 173, 1–5.
- (6) Tan, H.; Chen, Q.; Chen, T.; Liu, H. Selective Adsorption and Separation of Xylene Isomers and Benzene/Cyclohexane with Microporous Organic Polymers POP-1. ACS Appl. Mater. Interfaces 2018, 10, 32717–32725.
- (7) Castillo, J. M.; Vlugt, T. J. H.; Calero, S. Molecular Simulation Study on the Separation of Xylene Isomers in MIL-47 Metal-Organic Frameworks. *J. Phys. Chem. C* **2009**, *113*, 20869–20874.
- (8) Finsy, V.; Verelst, H.; Alaerts, L.; De Vos, D.; Jacobs, P. A.; Baron, G. V.; Denayer, J. F. M. Pore-Filling-Dependent Selectivity Effects in the Vapor-Phase Separation of Xylene Isomers on the Metal-Organic Framework MIL-47. *J. Am. Chem. Soc.* **2008**, *130*, 7110–7118.
- (9) Peralta, D.; Barthelet, K.; Pérez-Pellitero, J.; Chizallet, C.; Chaplais, G.; Simon-Masseron, A.; Pirngruber, G. D. Adsorption and Separation of Xylene Isomers: CPO-27-Ni vs HKUST-1 vs NaY. *J. Phys. Chem. C* **2012**, *116*, 21844–21855.
- (10) Minceva, M.; Rodrigues, A. E. Understanding and Revamping of Industrial Scale SMB Units for *p*-Xylene Separation. *AIChE J.* **2007**, 53, 138–149.
- (11) Minceva, M.; Rodrigues, A. E. Modeling and Simulation of a Simulated Moving Bed for the Separation of *p*-Xylene. *Ind. Eng. Chem. Res.* **2002**, *41*, 3454–3461.
- (12) Silva, M. S. P.; Moreira, M. A.; Ferreira, A. F. P.; Santos, J. C.; Silva, V. M. T. M.; Sá Gomes, P.; Minceva, M.; Mota, J. P. B.; Rodrigues, A. E. Adsorbent Evaluation Based on Experimental Breakthrough Curves: Separation of *p*-Xylene from C8 Isomers. *Chem. Eng. Technol.* **2012**, *35*, 1777–1785.
- (13) Rasouli, M.; Yaghobi, N.; Allahgholipour, F.; Atashi, H. Paraxylene Adsorption Separation Process Using Nano-Zeolite Ba-X. Chem. Eng. Res. Des. 2014, 92, 1192–1199.
- (14) Lachet, V.; Buttefey, S.; Boutin, A.; Fuchs, A. H. Molecular Simulation of Adsorption Equilibria of Xylene Isomer Mixtures in Faujasite Zeolites. A Study of the Cation Exchange Effect on Adsorption Selectivity. *Phys. Chem. Chem. Phys.* **2001**, *3*, 80–86.
- (15) Furukawa, H.; Cordova, K. E.; O'Keeffe, M.; Yaghi, O. M. The Chemistry and Applications of Metal-Organic Frameworks. *Science* **2013**, *341*, 974.
- (16) Moreira, M. A.; Santos, J. C.; Ferreira, A. F. P.; Loureiro, J. M.; Ragon, F.; Horcajada, P.; Yot, P. G.; Serre, C.; Rodrigues, A. E. Toward Understanding the Influence of Ethylbenzene in *p*-Xylene Selectivity of the Porous Titanium Amino Terephthalate MIL-125(Ti): Adsorption Equilibrium and Separation of Xylene Isomers. *Langmuir* **2012**, *28*, 3494–3502.
- (17) Vermoortele, F.; Maes, M.; Moghadam, P. Z.; Lennox, M. J.; Ragon, F.; Boulhout, M.; Biswas, S.; Laurier, K. G.; Beurroies, I.; Denoyel, R.; Roeffaers, M.; Stock, N.; Dueren, T.; Serre, C.; De Vos, D. E. p-Xylene-Selective Metal-Organic Frameworks: A Case of Topology-Directed Selectivity. *J. Am. Chem. Soc.* **2011**, *133*, 18526—18529.
- (18) Jin, Z.; Zhao, H.-Y.; Zhao, X.-J.; Fang, Q.-R.; Long, J. R.; Zhu, G.-S. A Novel Microporous MOF with the Capability of Selective Adsorption of Xylenes. *Chem. Commun.* **2010**, *46*, 8612–8614.
- (19) Torres-Knoop, A.; Krishna, R.; Dubbeldam, D. Separating Xylene Isomers by Commensurate Stacking of *p*-Xylene within Channels of MAF-X8. *Angew. Chem., Int. Ed.* **2014**, *53*, 7774–7778. (20) Alaerts, L.; Kirschhock, C. E.; Maes, M.; van der Veen, M. A.; Finsy, V.; Depla, A.; Martens, J. A.; Baron, G. V.; Jacobs, P. A.; Denayer, J. E. M.; De Vos, D. E. Selective Adsorption and Separation of Xylene Isomers and Ethylbenzene with the Microporous

- Vanadium(IV) Terephthalate MIL-47. Angew. Chem., Int. Ed. 2007, 46, 4293-4297.
- (21) ZareKarizi, F.; Joharian, M.; Morsali, A. Pillar-Layered MOFs: Functionality, Interpenetration, Flexibility and Applications. *J. Mater. Chem. A* **2018**, *6*, 19288–19329.
- (22) Xu, Y.-L.; Gao, Q.; Zhao, M.; Zhang, H.-J.; Zhang, Y.-H.; Chang, Z. Impact of the Flexibility of Pillar Linkers on the Structure and  $CO_2$  Adsorption Property of "Pillar-Layered" MOFs. *Chin. Chem. Lett.* **2017**, 28, 55–59.
- (23) Senthilkumar, S.; Goswami, R.; Obasi, N. L.; Neogi, S. Construction of Pillar-Layer Metal-Organic Frameworks for  $\rm CO_2$  Adsorption under Humid Climate: High Selectivity and Sensitive Detection of Picric Acid in Water. ACS Sustainable Chem. Eng. 2017, 5, 11307–11315.
- (24) Chen, Y.; Wu, H.; Yuan, Y.; Lv, D.; Qiao, Z.; An, D.; Wu, X.; Liang, H.; Li, Z.; Xia, Q. Highly Rapid Mechanochemical Synthesis of a Pillar-Layer Metal-Organic Framework for Efficient CH4/N2 Separation. *Chem. Eng. J.* **2020**, 385, 123836.
- (25) Wu, H.; Yuan, Y.; Chen, Y.; Xu, F.; Lv, D.; Wu, Y.; Li, Z.; Xia, Q. Efficient Adsorptive Separation of Propene over Propane through a Pillar-Layer Cobalt-Based Metal-Organic Framework. *AIChE J.* **2020**, *66*, 1–8.
- (26) Chen, Y.; Wu, H.; Lv, D.; Yuan, N.; Xia, Q.; Li, Z. A Pillar-Layer Metal-Organic Framework for Efficient Adsorption Separation of Propylene over Propane. Sep. Purif. Technol. 2018, 204, 75–80.
- (27) Hu, Y.; Zhang, W.; Zhang, X.; Wang, Z.; Li, Y.; Bai, J. Two Corrugated 2D Bilayer (63)(658) Topological Coordination Polymers: Synthesis, Structure, and Water-Induced Reversible Transformation. *Inorg. Chem. Commun.* 2009, 12, 166–168.
- (28) Barton, B.; Caira, M. R.; de Jager, L.; Hosten, E. C. N,N''-Bis(9-phenyl-9-thioxanthenyl)ethylenediamine: Highly Selective Host Behavior in the Presence of Xylene and Ethylbenzene Guest Mixtures. *Cryst. Growth Des.* **2017**, *17*, 6660–6667.
- (29) Lee, C. Y.; Bae, Y.-S.; Jeong, N. C.; Farha, O. K.; Sarjeant, A. A.; Stern, C. L.; Nickias, P.; Snurr, R. Q.; Hupp, J. T.; Nguyen, S. T. Kinetic Separation of Propene and Propane in Metal-Organic Frameworks: Controlling Diffusion Rates in Plate-Shaped Crystals via Tuning of Pore Apertures and Crystallite Aspect Ratios. *J. Am. Chem. Soc.* 2011, 133, 5228–5231.
- (30) Yang, L.; Liu, H.; Xing, J.; Yuan, D.; Xu, Y.; Liu, Z. Separation of Xylene Isomers in the Anion-Pillared Square Grid Material SIFSIX-1-Cu. *Chem. Eur. J.* **2021**, *27*, 6187–6190.
- (31) Perdew, J. P.; Burke, K.; Ernzerhof, M. Generalized Gradient Approximation Made Simple. *Phys. Rev. Lett.* **1996**, *77*, 3865–3868.
- (32) Borzehandani, M. Y.; Abdulmalek, E.; Rahman, M. B. A.; Latif, M. A. M. First-Principles Investigation of Dimethyl-Functionalized MIL-53(Al) Metal-Organic Framework for Adsorption and Separation of Xylene Isomers. *J. Porous Mater.* **2021**, *28*, 579–591.
- (33) Gee, J. A.; Zhang, K.; Bhattacharyya, S.; Bentley, J.; Rungta, M.; Abichandani, J. S.; Sholl, D. S.; Nair, S. Computational Identification and Experimental Evaluation of Metal-Organic Frameworks for Xylene Enrichment. *J. Phys. Chem. C* **2016**, *120*, 12075–12082.
- (34) Lannoeye, J.; Van de Voorde, B.; Bozbiyik, B.; Reinsch, H.; Denayer, J.; De Vos, D. An Aliphatic Copper Metal-Organic Framework as Versatile Shape Selective Adsorbent in Liquid Phase Separations. *Microporous Mesoporous Mater.* **2016**, 226, 292–298.
- (35) Pichon, C.; Methivier, A.; Simonot-Grange, M. H.; Baerlocher, C. Location of Water and Xylene Molecules Adsorbed on Prehydrated Zeolite BaX. A Low-Temperature Neutron Powder Diffraction Study. *J. Phys. Chem. B* **1999**, *103*, 10197–10203.
- (36) Mellot, C.; Simonot-Grange, M. H.; Pilverdier, E.; Bellat, J. P.; Espinat, D. Adsorption of Gaseous *p* or *m*-Xylene in BaX Zeolite: Correlation between Thermodynamic and Crystallographic Studies. *Langmuir* 1995, 11, 1726–1730.
- (3<sup>7</sup>) Cui, X.; Chen, K.; Xing, H.; Yang, Q.; Krishna, R.; Bao, Z.; Wu, H.; Zhou, W.; Dong, X.; Han, Y.; Li, B.; Ren, Q.; Zaworotko, M. J.; Chen, B. Pore Chemistry and Size Control in Hybrid Porous Materials for Acetylene Capture from Ethylene. *Science* **2016**, *353*, 141–144.